Project No. 10-918

Precursor Derived Nanostructured Si-C-X Materials for Nuclear Applications

Reactor Concepts
Mission Relevant Investigator Initiated Research

Dr. Rajendra Bordia
University of Washington

In collaboration with:
Purdue University
Pacific Northwest National Laboratory

Sue Lesica, Federal POC
Yutai Katoh, Technical POC

NEUP Nuclear Energy University Programs
U.S. Department of Energy

FINAL REPORT (OCTOBER 2010 – SEPTEMBER 2014)

Project No. 10-918: Precursor Derived Nanostructured Si-C-X Materials for Nuclear Applications

Investigators: Bordia, University of Washington (PI); Tomar ,Purdue University (Co-PI); Henager, Jr., PNNL (Co-PI)

ABSTRACT

Polymer derived ceramic route is an attractive approach to make structural materials with unique nanostructures that have very desirable high temperature properties. Processing techniques to make a variety of needed shapes and forms (e.g. coatings, matrices for fiber reinforced composites, porous ceramics) have been developed. With appropriate high temperature processing, the precursors can be converted to nano-crystalline materials.

In this collaborative project, we investigated the processing, stability and properties of nanostructured Si-C materials, derived from polymeric precursors, and their performance under conditions appropriate for nuclear energy applications. All the milestones of the project were accomplished. Some of the results are being currently analyzed and additional papers being prepared in which support from NEUP will be acknowledged. So far, eight peer-reviewed papers have been published and one invention disclosure made. In this report, we summarize the major findings of this project.

PROJECT OBJECTIVE

The overall goal of this project is to investigate the processing, stability and properties (thermal, mechanical, and storage) of nanostructured Si-C materials, derived from polymeric precursors, and their performance under conditions appropriate for nuclear energy applications. The specific objectives of the project are:

- To investigate the effect of precursor stoichiometry and processing conditions (e.g. temperature) on the resulting nanostructure. The thermo-mechanical stability of the nanostructure will also be investigated.
- To investigate the effect of the nanostructure on the mechanical and thermal properties.
- To investigate, experimentally and using simulations, the effect of irradiation on the stability of the nanostructure, and post irradiation thermal stability and mechanical properties.
- To experimentally and computationally investigate the ability of these materials to store and retain inert gas fission products.

SUMMARY OF THE RESEARCH CONDUCTED

During the project, work was conducted on the following tasks and the important results are summarized under each task.

TASK 1: PROCESSING AND STABILITY OF NANOSTRUCTURED SI-C CERAMICS

The goal of this task is to investigate the effect of precursor chemistry and processing parameters on the nanostructure of the ceramics. An additional goal is the investigation of the stability of the nanostructure as a function of temperature and external stresses.

In this project, under the supervision of the PI (Bordia at University of Washington), research has been conducted in the following areas of relevance to this task

Sub-Task 1.1: Effect of Stoichiometry and Temperature on the Nanostructure and Phases in Si-C

Under the supervision of the PI (Bordia at University of Washington) and co-PI (Henager, PNNL) research has been focused on Sub-Task 1.1 (Effect of Stoichiometry and Temperature on the Nanostructure and Phases of SiC). This work was completed through international collaborations with the Institute of Inorganic Chemistry, Bratislava, Slovakia and the Technology Institute in Vienna, Austria. The international collaboration was funded in part by the International Center for Materials Research Travel Grant to densify the amorphous SiC powders via hot pressing. The characterization of the SiC was done at the University of Washington Seattle and the Pacific Northwest National Laboratory.

Effect of crosslinking temperature on ceramic yield

It is understood crosslinking preceramic polymers has an effect on the final ceramic yield. In order to establish crosslinking protocols for the allylhydridopolycarbosilane preceramic polymer (SMP-10) (Fig. 1) it was thermally crosslinked at both 350°C and 400°C for two hours in the presence of 1 wt % dicumyl peroxide (a crosslinking agent).

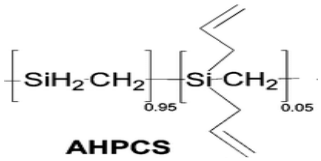

Figure 1. Allylhydridopolycarbosilane (SMP-10)

The ceramic yield of the crosslinked specimens was analyzed using thermogravimetric analysis (TGA) (STA 409C, Netzsch, Selb, Germany). It can be observed that the higher crosslinking temperature results in an increase ceramic yield (Fig. 2).

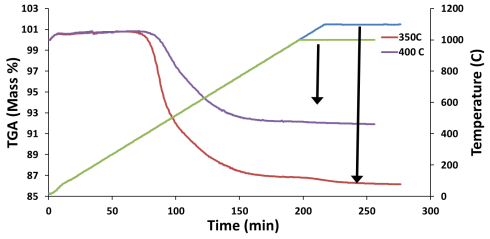

Figure 2. Ceramic yield increases with crosslinking temperature

It is clearly identified that samples crosslinked at lower temperatures have increased mass loss at lower temperatures and thus decreased ceramic yield. The final ceramic yield is 86% and 92% for the 350 °C and the 400°C crosslinked samples respectively. For the sample with the higher crosslinking temperature, the mass loss is complete at about 800°C. Based on these experiments, a crosslinking temperature of 400°C and pyrolysis temperature of 900°C was employed for processing the amorphous SiC powders. The crosslinking temperature assured an increase in crosslinks amongst the polymer chains to avoid increased mass loss. The final pyrolysis temperature of 900°C was necessary in the removal of all excess oligomers and monomers.

Boron modified SMP-10

Boron was added to SMP-10 by adding 1 wt% Decaborane to the liquid polymer in an inert glove box. The sample was then sonicated for 2 hours in order to evenly disperse the solid decaborane. The boron doped SMP-10 was thermally crosslinked to 400°C under gettered argon for two hours. Once removed from the furnace the crosslinked polymer was placed in a high energy ball mill for 60 minutes (Spex Mixer/Mill 8000M Spex SamplePrep, Metuchen, NJ, USA). The finely milled crosslinked samples were then transferred to the tube furnace for pyrolysis.

It can be observed through the XRDs (Fig. 3 & 4) that the boron-modified precursor is slightly more resistant to crystallization than is the unmodified precursor. This is an important finding of this project and is consistent with the SiBCN literature that suggests introduction of boron to the polymeric system provides a barrier to nucleation of the crystals.

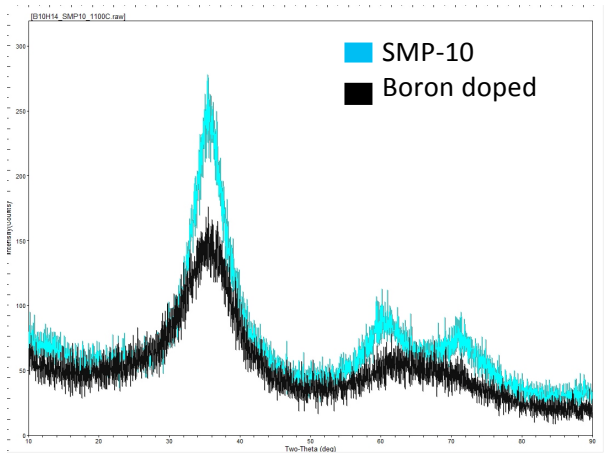

Figure 3. SMP-10 vs. B-SMP-10, 1100°C

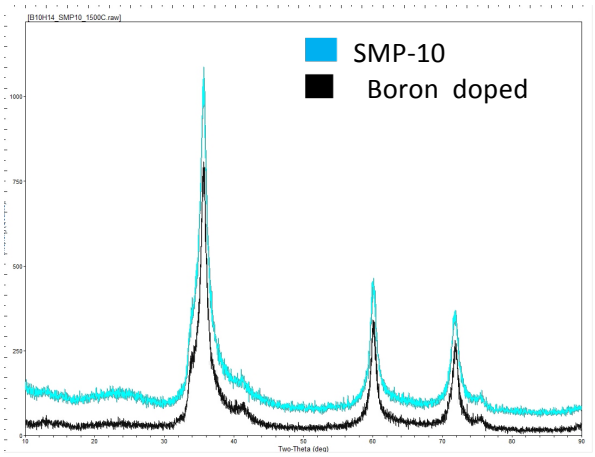

Figure 4. SMP-10 vs. B-SMP-10, 1500°C

Thermogravimetric Analysis (TGA) on Modified SMP-10

Dicumyl peroxide (dp) is a common crosslinking initiator in PDCS. Its effects on preventing the release of excess hydrocarbons during pyrolysis studied using thermogravimetric analysis. Decaborane is commonly used in the polymer derived ceramics (PDC) community to increase the amorphous stability in SiBCN PDCs. In this study the TGA of SMP-10 modified with decaborane and dicumyl peroxide (dp) separately was explored to understand the effects of final ceramic yield after pyrolysis.

The SMP-10 modified with 1 wt% decaborane was added directly to the SMP-10 liquid polymer and sealed in a scintillation vial in the presence of an inert glovebox, followed by sonication for two hours. The sample of SMP-10 modified with 1 wt% dicumyl peroxide was added in the same manner as above. The samples were then placed in the TGA using the heating rate shown in (Fig. 5)

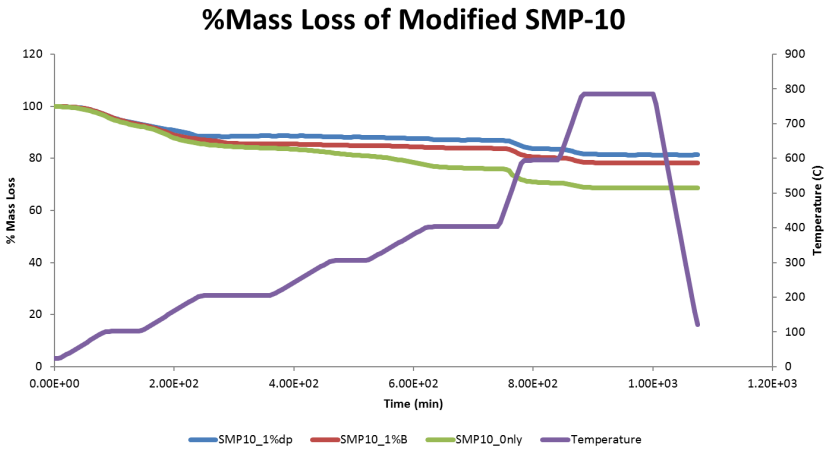

Figure 5. Ceramic yield of SMP-10 and additives

The TGA shows that SMP-10 alone without any modifications experiences a ceramic yield of 68 %, whereas when SMP-10 is modified with decaborane it achieves a ceramic yield of 78% and SMP-10 combined with the dicumyl peroxide catalyst achieves a ceramic yield of 82%. While these results were useful in decreasing mass loss from processing amorphous SiC powders, they will also be useful in the development of SiC coatings and additionally for SiC joining applications.

Preparation of SiC and SiBC powders for hot pressing

Powders containing varying weight percent of carbon, both with and without boron (sintering aid) were prepared in adequate quantities to study the radiation and mechanical properties of the SiBC and SiC materials. The samples containing excess carbon in the SMP-10 precursor were prepared through molecular modifications with DVB in 0, 1 & 5 wt%. After DVB addition, the samples were crosslinked under gettered argon to 400° C for two hours. The crosslinked samples were then milled using a Spex mill to obtain fine powders. After milling the crosslinked samples to a fine powder they were pyrolyzed to 900°C for two hours. In addition to the 1-5 wt% of DVB, boron was introduced using decaborane at 1wt% in the samples for use a sintering aid during hot pressing.

In order for the samples to achieve their maximum theoretical density during hot pressing, it is necessary to thoroughly mill them to a very fine particle size. As such, the 0-5 wt% excess carbon SiC samples were milled using an attrition mill (Szegvari Attritor). This was accomplished using 750 grams of 5 mm SiC milling media, followed by a Si_3N_4 attritor arm in a 750 mL Teflon lined vessel. The samples were all milled for 2 hours at 400 rpm in the presence of 200 mL of hexane. The samples were then removed and placed in a 1000 mL round bottom flask and placed in a rotovap (Heidolph laborata) at 40°C with a pressure of 335 mbar to remove all of the hexane from the finely milled powder. The pressure from the rotovap was slowly decreased as more of the hexane was removed from the sample. After much of the hexane was removed from the sample it was then placed in a Vacucell BMT vacuum oven, heated to 80°C under a pressure of ~200 mbar and left overnight to fully evaporate off the hexane. The sample was then sieved for 15 minutes at a time with 20-second intervals until all of the powder went first through a 125 µm sieve containing about fifteen 5 mm SiC media balls followed by the 71 µm sieve also containing about fifteen 5 mm SiC media balls and into the final collection pan. The following samples have been milled to submicron particle sizes:

Table 1. SMP-10:C powdered samples prepared for hot pressing

%DVB	Temp °C	Decaborane
0	800	0 wt%
1	800	0 wt%
3	800	0 wt%
5	800	0 wt%
0	800	1 wt%
1	800	1 wt%
3	800	1 wt%
5	800	1 wt%

Additionally, particle size analysis was done on all of the milled powders and all maintained particle sizes below 700 nm.

Exploration of Conversion to Ceramic

One possible use of polymer derived ceramics in nuclear applications is their use as matrix materials for fiber reinforced ceramic matrix composites. It is observed in the literature that after pyrolysis of SMP-10 there is a tendency to have an excess quantity of Si. We have since prepared samples to finely tune a 1:1 Si/C ratio by adding divinylbenzene (DVB) in quantities from 0-5 wt% to allylhydridopolycarbosilane (SMP-10) from Starfire Systems. The various samples were heat treated using a one step pyrolysis method in gettered argon to 800°C using the thermal profile shown in Fig. 6.

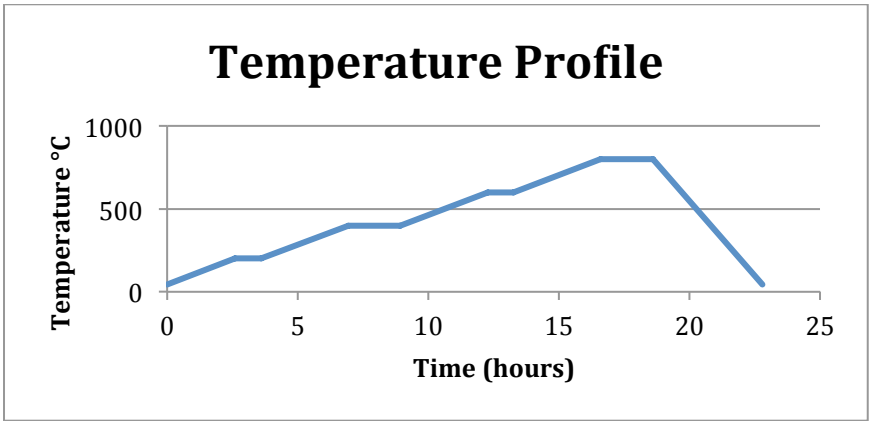

Figure 6. One step pyrolysis heating profile

We then crystallized the samples at temperature up to 1500°C and density measurements were taken before and after this calcination. The density of the samples pyrolyzed at 800 and 1500°C were 69 and 73% respectively. SEM imaging of the 1 wt% excess carbon shows tunnels leftover from hydrocarbon evolution during pyrolysis at both 800 and 1500°C in (Fig 7 & 8) below.

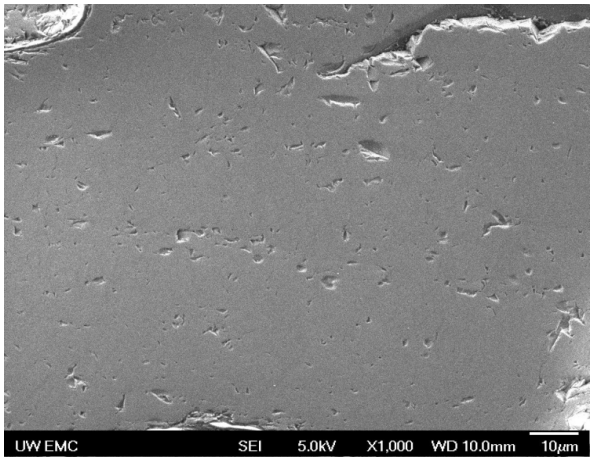

Figure 7. Pyrolysis of SMP-10 at 800°C

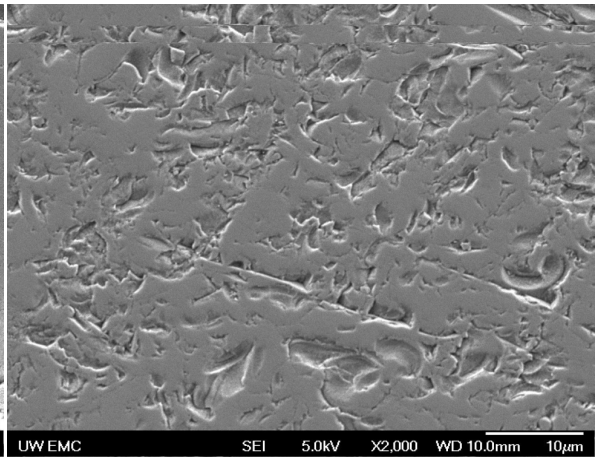

Figure 8. Pyrolysis of SMP-10 at 1500°C

Foamed SiC

Another objective of this project was to make porous SiC materials as possible storage systems for radioactive gases. Foaming with azodicarbonamide (ADA), a nitrogen based compound Fig. 9, was investigated to make a porous polymeric structure. Utilizing this method in preceramic polymers is a novel method for the development of porous SiC for nuclear applications. This method controllably introduces pores into the system that are unattainable through traditional ceramic processing routes.

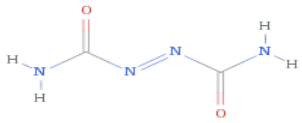

Figure 9. Azodicarbonamide molecular structure

When heat-treated, it allows for the decomposition of the ADA and thus leaves behind a porous structure. The ADA was added to SMP-10 in weight percentages of 0, 1, 3, and 5 wt. %. The mixtures were sealed within a N_2 pure glovebox and placed in an ultrasonic bath for 2 hours. As shown in Fig. 10 ADA thermally decomposes completely at 200°C by release of nitrogen gas.

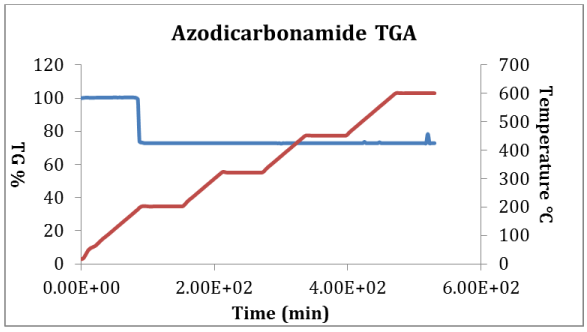

Figure 10. Decomposition of ADA w/ temperature

The following processing protocols have been developed for the formation of foamed SiC structures using azodicarbonamide in conjunction with decaborane and also “free carbon”.

I) Dispersing ADA
II) Determination of optimal holding temperature during foaming
III) Decaborane in foamed SiBC
IV) Determination of optimal ramp rate for foaming
V) ADA concentration in foamed SiBC
VI) Divinylbenzene addition for samples containing excess carbon in foamed SiBC

Dispersing ADA

In the literature ADA is most commonly dispersed in liquid precursors by stirring for ~24 hours. This approach was pursued in this work along with dispersion through ultrasonication of ADA in the liquid SMP-10. The distribution of ADA within the system was accomplished by adding 1 wt% ADA to the SMP-10 precursor followed by stirring for 24 hours or ultrasonication for 2 hours, in the presence of nitrogen. A new finding of this study is that the samples in which ADA was stirred into the system had a gradient of porosity due to uneven dispersion. Whereas, the samples that were ultrasonicated had a uniform distribution of pores within the system.

Viscosity of the colloidal system was additionally considered while distributing ADA into the SMP-10 precursor. This was accomplished with the addition of a 1:5 wt. ratio (Hexane:SMP-10) followed by the addition of 1 wt% ADA in SMP-10. This was done to determine the role of viscosity in foaming SMP-10. Hexane provided a means of further increasing the separation of ADA particles in the SMP-10. The remainder of the ADA foaming parameters below all use a 1:5 ratio of Hexane:SMP-10 and ultrasonication for two hours while sealed within a N_2 pure glovebox.

Foaming Temperature

ADA decomposes at 200 °C releasing nitrogen in the process thus causing foaming. Therefore the 200°C temperature is a typical holding temperature in foaming of the polymer derived ceramics. 200°C is utilized as a start for foaming SMP-10 and holding for two hours to complete off gassing of the ADA. The SMP-10 is a liquid polymer and it can be understood that the foaming properties of the PDC is precursor dependent thus holding temperature for each precursor will need to be modified as needed.

After dispersion of ADA into the system, the sample was placed in the furnace and the foaming temperature was varied (200, 250, 300°C) and held for two hours at a time under gettered argon. Based on quality of the foam, a holding temperature of 300°C for two hours was utilized for the remainder of the foaming studies since this produced samples with the most uniform porous structure. The foamed polymeric samples were converted to ceramic by heat treatment at a temperature of 900° C.

Effects of heating rate

In the literature a very slow ramp rate (1-3 °C/min) is most commonly used when foaming PDCs. However, as noted previously, the foaming rates are precursor dependent, with the majority of the literature utilizing solid precursors in the development of porous monoliths. Because this research utilizes a liquid precursor, a variety of heating rates were explored for the foaming process. A mixture of ultrasonicated SMP-10 with Hexane (1:5 Hexane:SMP-10 wt. ratio) and 1 wt. % ADA was heated at 1, 2, 3, 5, 10 , and 20 °C/min to 300 ˚C in gettered argon Fig. 11.

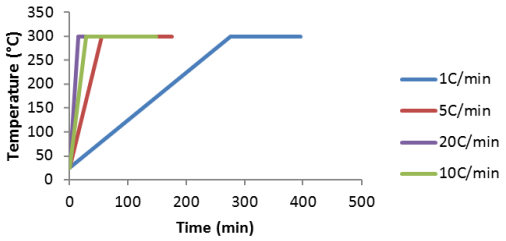

Figure 11. Heating rates explored for the foaming of allylhydridopolycarbosilane

Slow heating rate (1-5°C/min causes inadequate release of gases during crosslinking of the polymer leading to destruction of the monolith. Very fast heating rate (20C/min) leads to directional porosity from decomposition of the ADA very quickly Fig. 12.

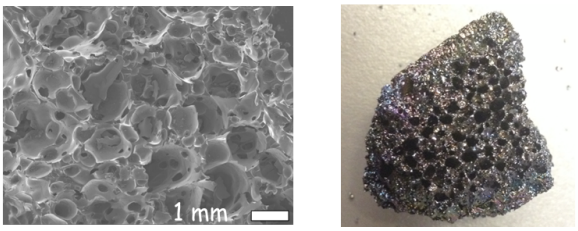

Figure 12. 20°C/min led to directional porosity for removal of decomposing ADA

A heating rate of 10°C/min proved to be an ideal method in obtaining a uniform distribution of pores in the monolith Fig. 13.

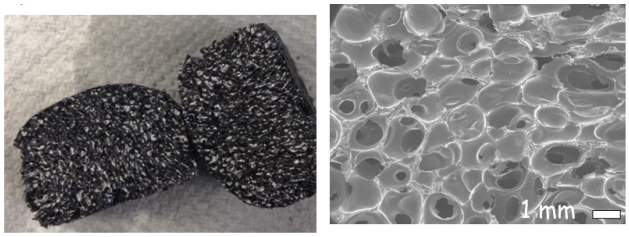

Figure 13. 10°C/min yielding uniform distribution of pores

Effect of the foaming modifier

The foaming modifier (decaborane) was a necessity in this process due to large deleterious pores forming in the center of the monolith from coalescence of gas bubbles during curing in the absence of a foam modifier (Fig 14.a).

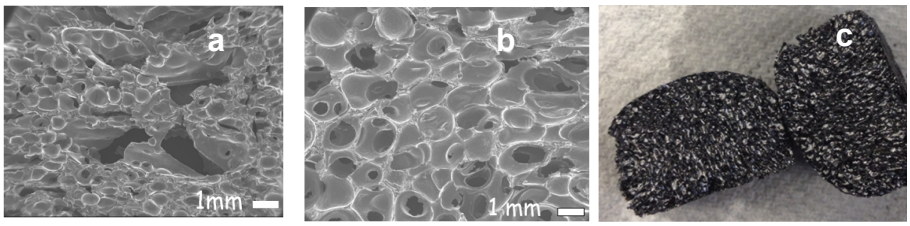

Figure 14. a) 1 wt% ADA, 0% decaborane b & c) 1 wt% ADA, 1 wt% decaborane

It can be observed that the hydroboration reaction of decaborane with SMP-10 alters the curing of the system such that a uniform distribution of pores is maintained (Fig. 14.b and c). The pore morphology of the boron-modified SMP-10 system was tailored by varying the concentration of decaborane. This method of foaming produced porous SiC monoliths with a controllable trend from elliptical to spherical pores as the amount of decaborane increases (Fig 15).

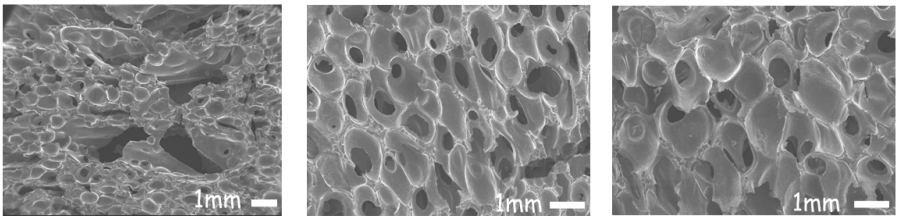

Figure 15. 0, 0.5 and 1.5% decaborane (respectively) added to 1 wt % ADA

It can also be appreciated that although decaborane assists with foaming, it itself is not a foaming agent as can be observed in Fig. 16. Here it can be seen thatin samples without ADA (the foaming agent), a very non uniform foam with large concentration of cracks is produced.

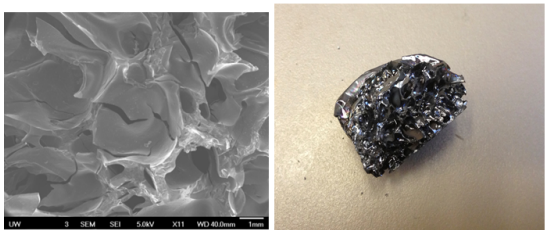

Figure 16. Decaborane and no ADA

The Effect of ADA concentrations

The effect of ADA (0.1, 0.3 & 5 wt% ADA) was also explored in the direct foaming of SMP-10 modified with 1 wt% decaborane. In contrast to increasing the concentration of decaborane, increasing the foaming agent ADA yielded a decrease in pore size and a change in pore morphology from spherical to ellipsoidal (Fig. 17).

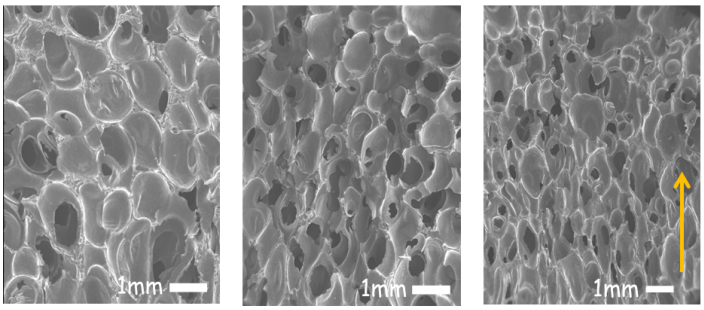

Figure 17. 0.1, 0.3 & 5 wt% ADA, very little ADA is necessary to foam the SMP-10

Modifications with Divinylbenzene

A final modification of the SMP-10 precursor was with excess carbon in the form of divinylbenzene. This was done to investigate the effect of precursor stoichiometry (specifically C/Si). The quantity of DVB used allowed for fine tuning of the free carbon introduced into the system. Previous studies involving SiOC PDCs have shown that when precursors are converted to ceramics, the excess carbon forms homogeneously dispersed graphene layers with nano-domains estimated at 1 to 5 nm (Fig 18). [1] The amount of carbon in the precursor and the processing temperature leads to the formation of either turbostratic nanocarbon domains or percolating graphene stacks (for high carbon content)[2,3] (Fig. 19).

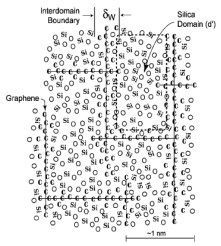

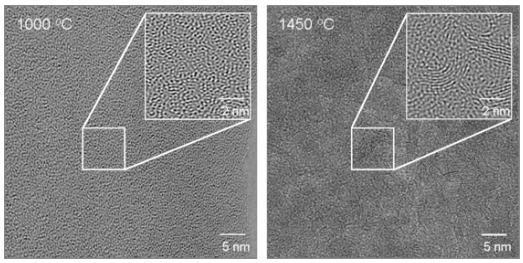

Figure 18. Schematic of graphene in SiOC PDCs[1]

Figure 19. Turbostratic SiOC w/ Temp[2]

In this research we aim to explore the resultant nanostructure of excess carbon on SiC PDCs and its properties. Here we have introduced various concentrations of divinylbenzene with 1 wt% ADA and 1 wt% decaborane. It was observed that the pore morphology is not altered through addition of excess carbon until very high concentrations of divinylbenzene have been introduced (Fig. 20).

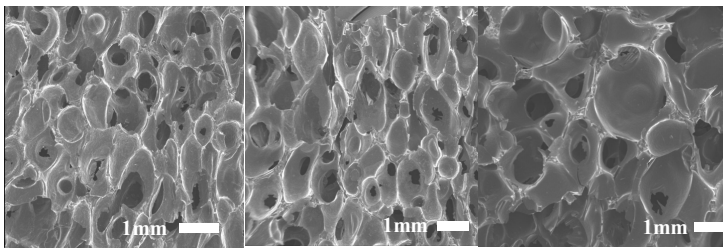

Figure 20. 1 wt% ADA, 1 wt% decaborane w/ 0, 5 & 10 wt % DVB in SMP-10 left to right

Therefore the effects of the “free carbon” phase introduced in this porous system from 0-5 wt% excess carbon can directly be compared.

This method of foaming allowed for a uniform distribution of pores to be obtained Fig. 21

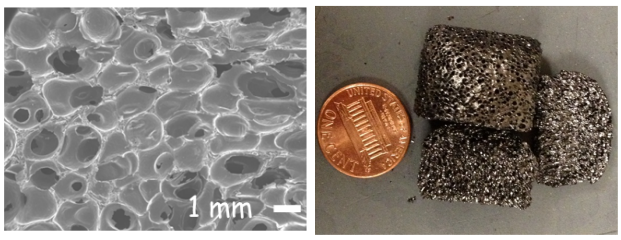

Figure 21. uniform distribution of pores

Future Work:

The proposed work in the project has been completed. However to fundamentally investigate the process, additional research needs to be conducted. Sepecifically, a few questions need to be answered and the graduate student Shelly Arreguin has applied for funding through the DAAD, to further advance this project. If awarded the funding through the DAAD, the specifics of the proposed research will continue as follows:

- Investigate the role of viscosity and stabilization of the polymer melt for the following processing variables: holding temperature, rate of curing, dispersal mechanism, colloidal system and concentration of foaming modifiers (decaborane & divinylbenzene) and foaming agent (ADA)
- Using TGA/FTIR determine the temperature and chemical nature of the evolved gaseous species leaving behind the porous monolith.
- Investigate the pore volume, surface area and densities of the variety of porous materials using mercury intrusion porosimetry.
- Experimentally determine the ability of these materials to store and retain gaseous products.
- Investigate the thermal properties of the varying pore morphologies and additionally the effect of the carbon nanodomains of the porous SiC ceramics
- Determine: pore density, pore and cell size distribution, connectivity and strut thickness distribution using μCT

References

(1) Saha, A.; Raj, R.; Williamson, D. Journal of the American Ceramic Society 2006, 89, 2188.
(2) Kleebe, H.; Blum, Y. *Journal of the European Ceramic Society* **2008**, *28*, 1037.
(3) Knight, D. S.; White, W. B. *Journal of Materials Research* **1989**, *4*, 385.

Sub-Task 1.2: Effect of Temperature and Stress on the Nanostructure and Phases in Si-C

Hot Pressing Amorphous SiC Powders

The amorphous submicron SiC powders were hot pressed to a temperature of 2050 °C and a pressure of 30 MPa in a 30 mm graphite die. The hot pressing was accomplished at the Technology University in Vienna, the following is the temperature/pressure regime that was optimized to densify the hot pressed SiC Fig. 22.

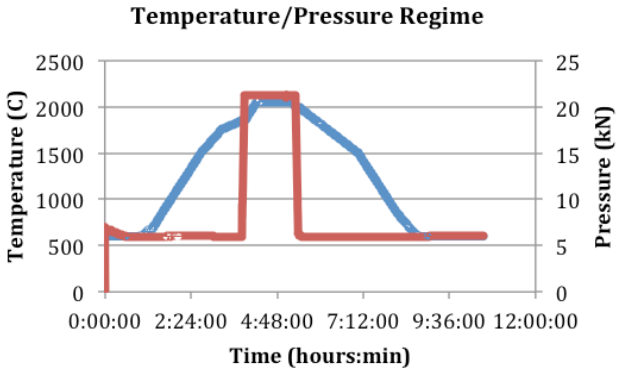

Figure 22. Temperature/Pressure profile for densification

Using Archimedes density measurements it can be observed that the samples without boron could not be sintered to high density. The samples with boron were densified to a density greater that 90 %. Thus it is clear that the molecularly added boron serves as a sintering aid. The samples with excess carbon resulted in slightly better densification as shown in Table 2.

Table 2. Hot pressed SiC samples

Sample	Bulk Density g/cm3	Theoretical Density
0 wt% C, 1 wt% B	2.96	92%
1 wt% C, 1 wt% B	3.02	93.9%
3 wt%C, 0 wt% B	1.95	61.3%
5 wt% C, 1 wt% B	3.205	99.9%
5 wt% C, 1 wt% B	3.14	97.8%
5 wt% C, 0 wt% B	2.20	68.6%

Characterization of the polymer derived SiC ceramics

Excess carbon was added in the form of divinylbenzene to the powders for the reasons presented in the porous section above. In this research, a graphene nanodomain was introduced into the SiC system through molecular modifications of the preceramic polymer utilizing divinylbenzene (DVB). The graphitic regions in this material have been explored using Raman spectroscopy. The G band indicates the presence of ordered graphitic regions, whereas the D band represents lack of lattice symmetry (Fig. 23).

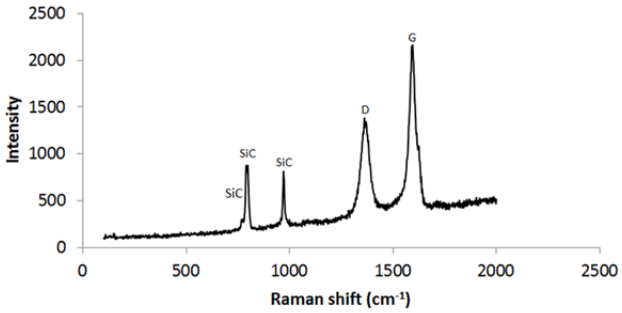

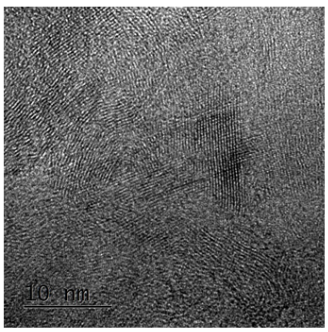

Figure 23.Confirmation of ordered carbon domains within the SiBC system and the appearance of turbostratic regions using TEM

XRD analysis of the SiC PDCs with temperature indicated that the 3C phase is the first polytype present during the amorphous to crystalline transition Fig. 24 .

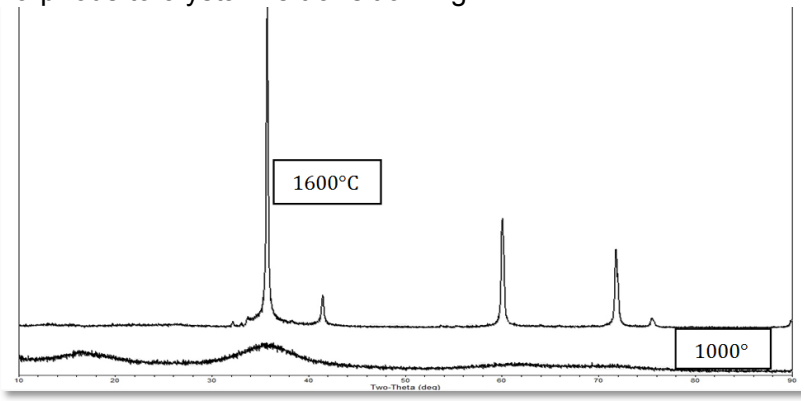

Figure 24. Amorphous to Crystalline transition and the presence of cubic SiC

Through characterization of the hot pressed SiC ceramics the 6H phase along with the 3C polytype is observed in the XRD in Fig. 25. The 3C polytype overlaps entirely with the peaks in the 6H phase, therefore additional characterization of the material is necessary to determine adequate ratios of the two phases present in these samples.

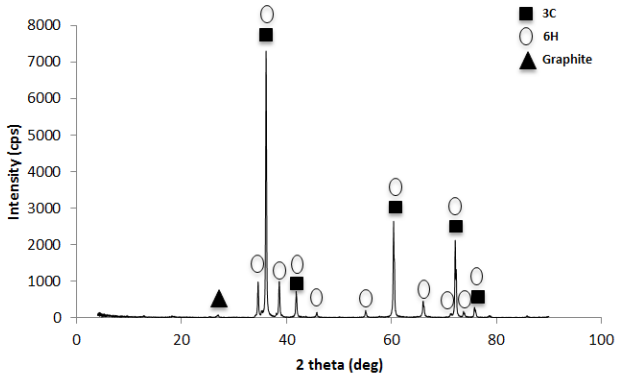

Figure 25. 3C and 6H polytypes present in hot pressed SiBC samples

SEM analysis has shown that elongated needle-like grains representative of abnormal grain growth are present in the hot pressed SiC samples. The elongated grains are indicative of a hexagonal polytype, more specifically 6H (determined from XRD analysis). It can be seen that with increasing concentration of carbon there is increasing concentration of the 6H phase Fig. 26. This is suggestive that the graphite nanodomains within the material are dictating the resultant polytype.

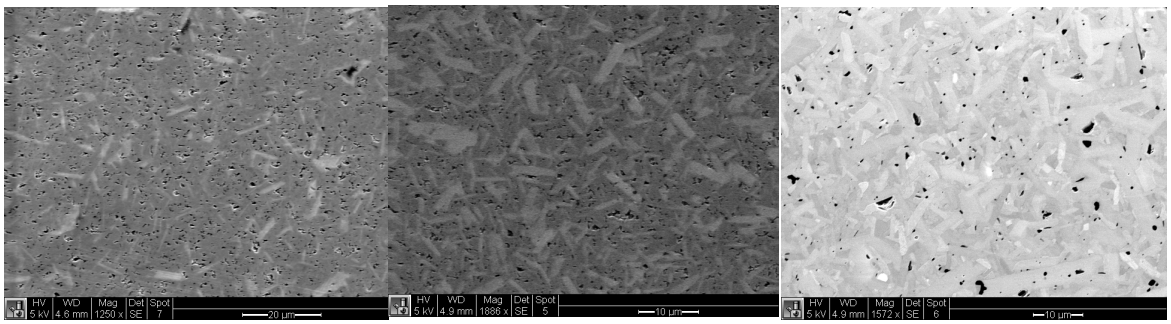

Figure 26. Microstructural evolution of SiC with excess carbon 0, 1 & 5 wt % (left to right)

The evolution of the 6H polytype with increasing carbon concentration can be further realized through ^{29}Si MAS NMR. Using ^{29}Si MAS NMR the polytypes present in the SiC samples can be effectively separated out. Here it can be seen that with increasing carbon concentration the 6H phase is stabilized at the expense of the 3C phase Fig. 27.

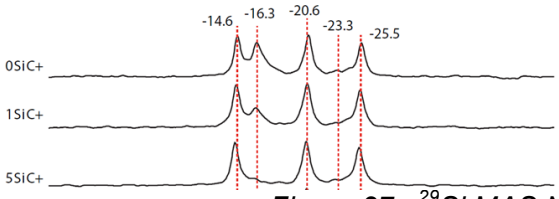

^{29}Si Chemical Shift			
	6H	3C	4H
A	-13.9		
B	-19.9		
C	-24.6		-23
	-16.1 or -18.3		

Figure 27. ^{29}Si MAS NMR of SiC

It can be appreciated that although boron is present in this system, the manner in which boron was introduced in this processing route did not dictate the resultant polytypes. This can be seen in the XRD in Fig. 28, indicating that either with or without boron the same phases are present in the polymer derived SiC samples are observed.

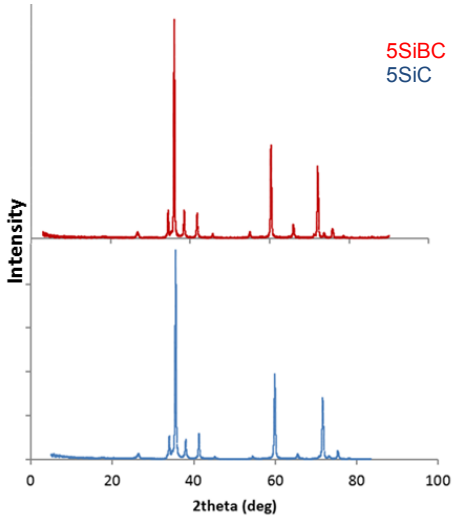

Figure 28. XRD of 5 wt% excess C w & w/o boron

Although, the polytypes are the same, without the use of boron as a sintering aid for the densification of SiC, there is not enough driving force for sintering to occur. This is displayed in Fig. 29 where a highly porous sample is observed and also in Table 2 where Archimedes density measurements indicate the very low theoretical density of the samples w/o boron addition.

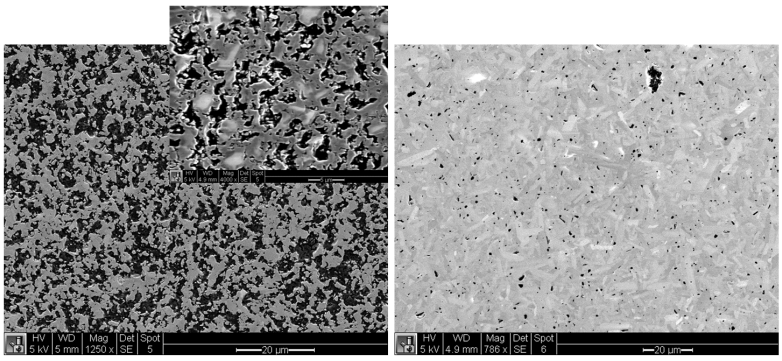

5wt% excess carbon in SiC, **no boron** 5wt% excess carbon in SiC, **1 wt% B**

Figure 29. Necessity of a sintering additive in the densification of SiC

Although use of boron as a sintering aid is not a new phenomenon, the method in which boron was introduced in this route was unique. In the literature, it is noted that when amorphous boron is milled in with SiC powders the impurity of the amorphous boron influences the polytypic phase present. It is well observed that this method of boron addition promotes the stabilization of the 4H polytype. Whereas, in this study boron modification to the preceramic polymer did not appear to dictate the resultant polytype, nor did it deliver the 4H polytype. It did however allow for the densification of SiC, which was not possible without the use of a sintering additive using this route.

The addition of amorphous boron to the submicron amorphous polymer derived silicon carbide samples was explored to compare with both literature and modified polymers. These studies showed that the this method produced the 4H phase observed in the literature Fig. 30. When utilizing the same composition, with boron modifications to the polymer, we observe 6H and 3C SiC (the same phases present without boron modifications). This is an important finding of this study and has fundmantal implications for the stability of the different SiC polytypes.

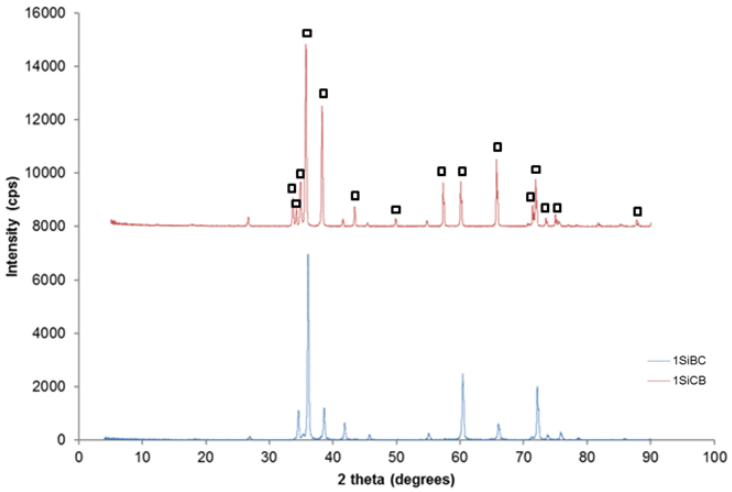

Figure 30. Polymeric modifications vs. powder modification w/ boron

Through SEM analysis we observe large elongated grains from the sample with amorphous boron added to the amorphous SiC PDC powders Fig. 31. There is clearly a significant difference in the resultant microstructure depending on how and when boron is added to the system. When compared

with the boron added molecularly (of the same composition) (Fig. 32) the system is composed of two phases a 3C matrix embedded with the 6H elongated grains, whereas when boron is added to the powder the system is composed of very large 4H SiC grains (Fig 31).

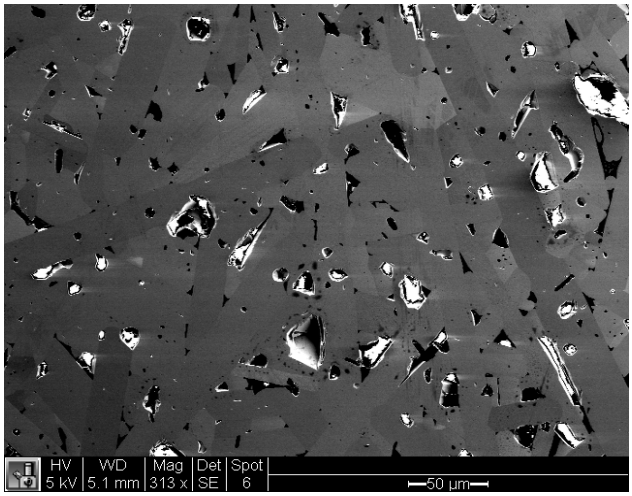

Figure 31. Amorphous boron in SiC (4H polytype)

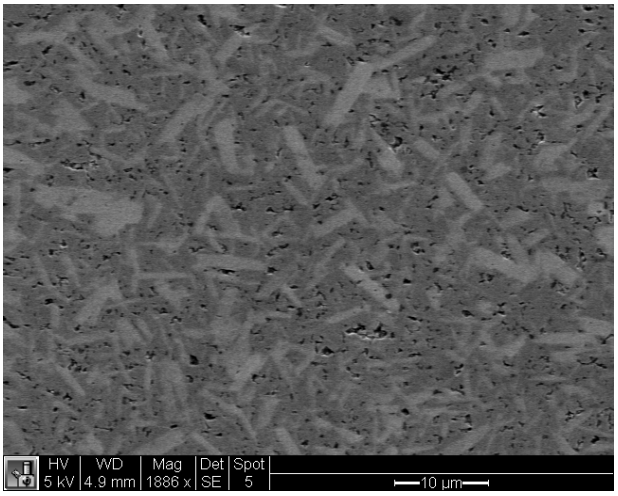

Figure 32. Polymer modifications w/ B (3C & 6H)

Using EMSL facilities at PNNL, ToF SIMS was used to observe the distribution of boron in the densified SiC samples. In the molecularly modified precursors, we can see that the boron is dispersed quite evenly in the sample, however when boron was introduced to the amorphous SiC powders the location of the boron is within the porous regions of the sample Fig. 33.

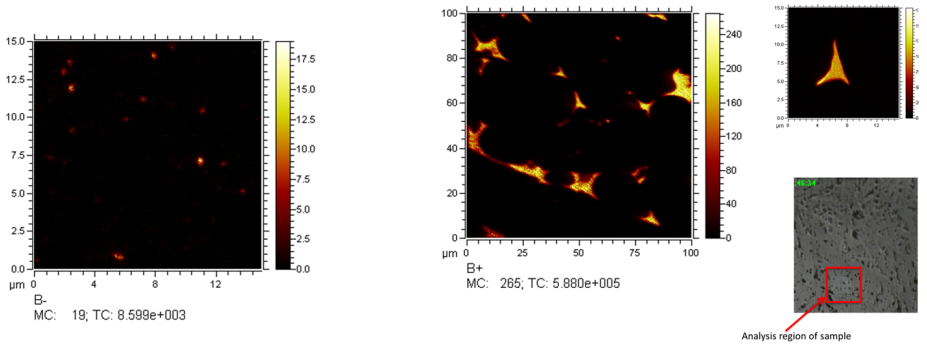

Figure 33. Boron distribution in modified polymers and powders (left to right respectively)

Using Nano-SIMS the elements most closely associated with boron and their locations relative to the microstructure could be observed. The SiC in which amorphous boron was added to the powder displayed a strong association with carbon and is suggestive that it is organized into a boron carbide phase represented by the magenta region in Fig. 34. The green region outside the boron carbide areas showed boron and silicon rich areas.

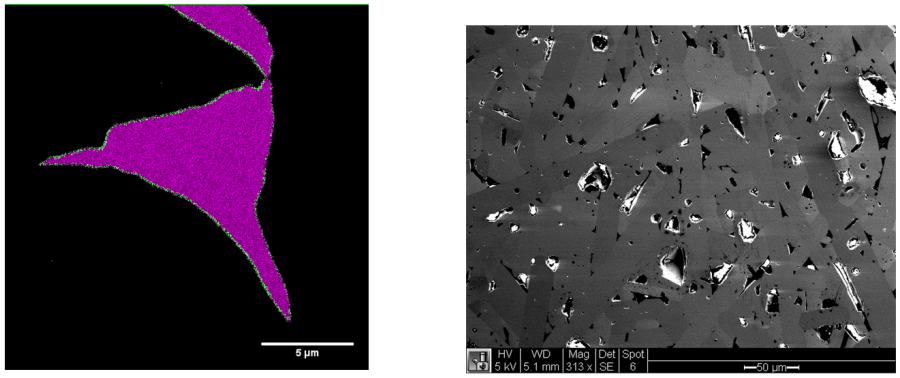

Figure 34. Nano-SIMS showing regions w/ increased B concentration and their association with Si & C

Using NanoSIMS to explore the regions of high boron concentration in samples in which boron was introduced to the polycarbosilane through a molecular process showed that boron is situated inside the SiC grains (as opposed to on the grain boundaries as is experienced when adding boron powder to SiC powder) Fig. 35.

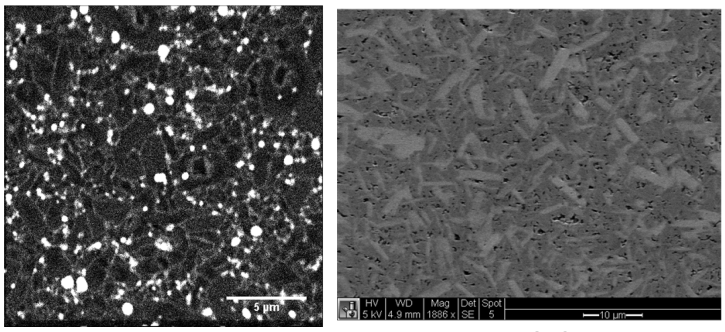

Figure 35. Boron located inside the SiC grains

Due to the unique manner in which boron is situated in this material there is possibility that the properties vary considerably in comparison to more traditional routes of solid state sintering SiC with B addition. When further locating boron, carbon and silicon rich regions in the molecularly modified precursors it can be observed that the boron again organizes with boron carbide as represented by the magenta regions and additionally that boron also has areas of silicon boride outside the boron carbide rich centers (represented by the white regions) Fig. 36. The red regions are representative of carbon rich areas in the sample.

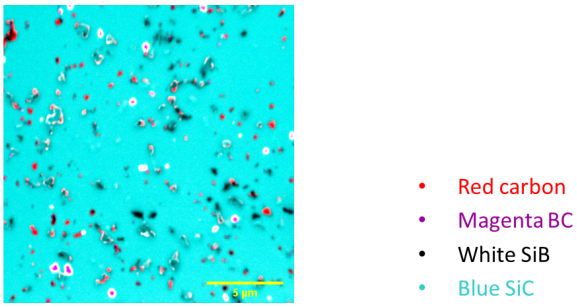

Figure 36, Boron modified precursor, showing organization of B & C in the structure

NanoSIMS analysis of modified precursors with excess carbon from 1 & 5 wt % show variability in the size distribution of the boron and carbon clusters Fig. 37. Here it can be observed that in the 1 wt% excess carbon in SiC the boron and carbon distribution is more dispersed, whereas with increasing carbon concentration there are larger clusters within the system. Due to both compositions having the same amount of boron in the system this is perhaps indicative that diffusion is faster during sintering with increasing carbon concentration.

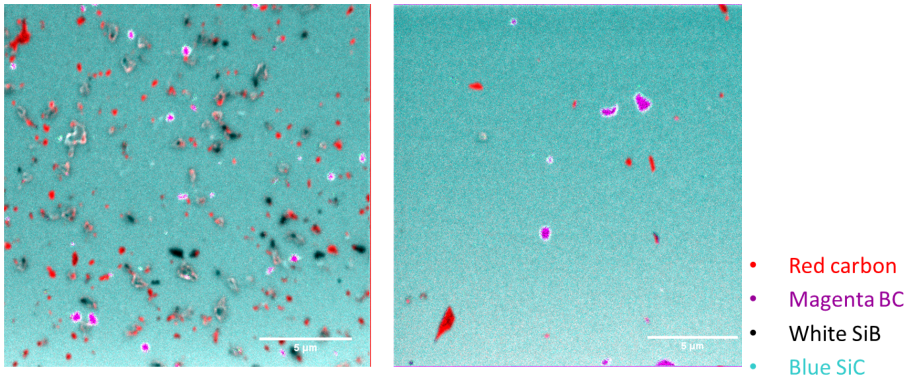

Figure 37. 1 wt% excess carbon and 5 wt% excess carbon (right to left)

Currently at PNNL, we are looking at 11B MAS NMR to determine the coordination chemistry of the boron in the matrix and TEM to observe locations and elements surrounding the boron. Using these characterization techniques we can develop better insight to how diffusion of atoms takes place when using boron as a sintering additive. Preliminary TEM results of the samples in which the polymeric phase was modified with boron, show that boron is located directly within the grains themselves (as opposed to being situated on the grain boundary). The intent is to better understand the sintering mechanisms taking place under the influence of boron addition.

TASK 2: MECHANICAL AND THERMAL PROPERTIES OF NANOSTRUCTURED SI-C CERAMICS

The goal of this task is to investigate the mechanical and thermal properties for the range of nanostructures produced. The goal is to develop a relationship between nanostructure and the mechanical properties of these materials.

We have measured the room temperature hardness, elastic modulus and the thermal diffusivities of the materials as a function of the composition and the nanostructure. In addition, the effect of irradiation on the mechanical properties has been measured.

The results are being currently analyzed. The results will be published with acknowledgement to NEUP funding.

TASK 3: RADIATION EFFECTS AND INERT GAS STORAGE ABILITY

The primary focus is to determine the stability of the nanostructure under irradiation and to determine the suitability of these materials for storing inert gas fission products. Both experimental and simulation research will be conducted.

Sub-Task 3.1: Experimental Studies on Radiation Effects

The focus of the task was on the design of the ion implantation experiments at PNNL. This was accomplished using SRIM & TRIM to simulate the depth of ion penetration and the amount of recoils. These

experiments were based on varying the type of ion, energy and angle with our SiC sample. The limits of the accelerator and length of the experiment were also taken into consideration with TRIM simulations. In the Fig. 38 & 39, gold ions were used for implantation due to their ability to induce more damage in a shorter period of time.

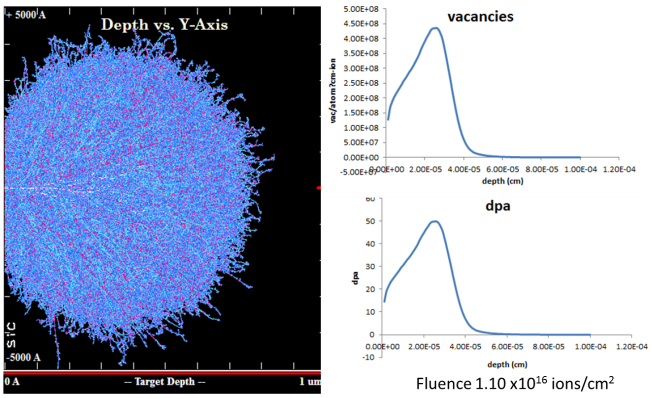

Figure 38. 2 MeV Au implantation

In these experiments we opted to utilize 5MeV such to induce more damage at greater depths in a shorter period of time Fig. 39.

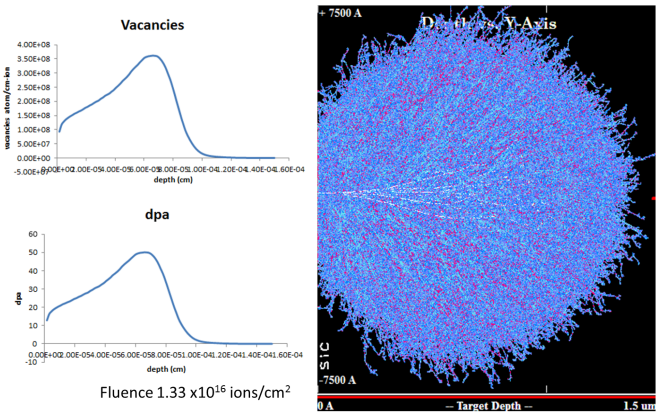

Figure 39. TRIM plot of 5 MeV

The implantation was done at 600C and the dpa at the surface was 20 and 2 dpa for 2 sets of samples. The samples included 3 samples in which boron was added at the molecular level and excess carbon in the amounts of 0, 1 & 5 wt%. In this set we also included the one sample in which boron was introduced to the powder vs. the polymer to show any variation in damage. Additionally, we masked off a region such that a portion of the sample did not experience any ion irradiation damage. Furthermore, we implanted ions for a short period of time at cryogenic temperatures so that we had low temperature irradiation damage such that AFM measurements could be accomplished more readily.

Future

The graduate student Shelly Arreguin will graduate prior to completing defect analysis of the irradiated samples using TEM and SAXS. She has applied for funding through the EAPSI NSF program to further this research. If awarded the funding she will travel to the Center for Microscopy and Microanalysis at the University of Queensland in Brisbane, Australia to:

- Explore the role of the carbon bonding & morphology in relation to SiC polytypes using TEM.

- Complete microstructural analysis of the various polytypes and graphene interfaces.
- Learn Techniques for Weak Beam method of TEM for analysis of ion-damaged samples. Analyze the nature of atomistic point defects in samples exposed to varying doses of ions
- Learn SAXS techniques. Determine size of nanodomains in samples processed under different conditions and with varying carbon content

Sub-Task 3.2: Computational Studies on Radiation Effects
This part of the project is being led by Prof. Tomar at Purdue. Several studies have been conducted. Specifically:

1. A program to generate a 3C-SiC structure has been developed by Co-PI research group (Tomar at Purdue University). The program is designed to generate 3C-SiC structure considering its structural information such as the lattice constant, the fractional coordinates, lattice orientation, and so on. Within the framework of density functional theory, the ab-initio quantum tensile simulation has been performed to investigate the effect of the direction of interface on the material strength using NWchem, the computational chemistry software. In this study, three different directions of interface (0^0, 45^0, 60^0) have been considered and simple tension was applied in z direction. The obtained results were used for the simulation to study the fracture behavior of nuclear materials such as crack initiation and propagation. Details of this investigation was presented in the First Annual report.

2. To investigate the effect of radiation damage at grain boundaries (GB) on the peak tensile strength of cubic silicon carbide (3C-SiC, also called β-SiC) has been examined using *ab initio* simulations. Three SiC nanostructure samples with different GB geometries were analyzed. Details of this investigation were presented in the Second Annual report.

Finally, the effect of SiC grain boundary configuration and graphene defect on tensile strength of epitaxial graphene (EG) on 3C-SiC nanostructures have been investigated. In this study, four different graphene defect types are considered along with three different 3C-SiC grain boundary configurations. The model systems are shown in Fig. 40. Cyan and yellow circles represent carbon (C) and silicon (Si) atoms, respectively. Figure (a) and (b) show the side and top views of EG on SiC analyzed in this work.

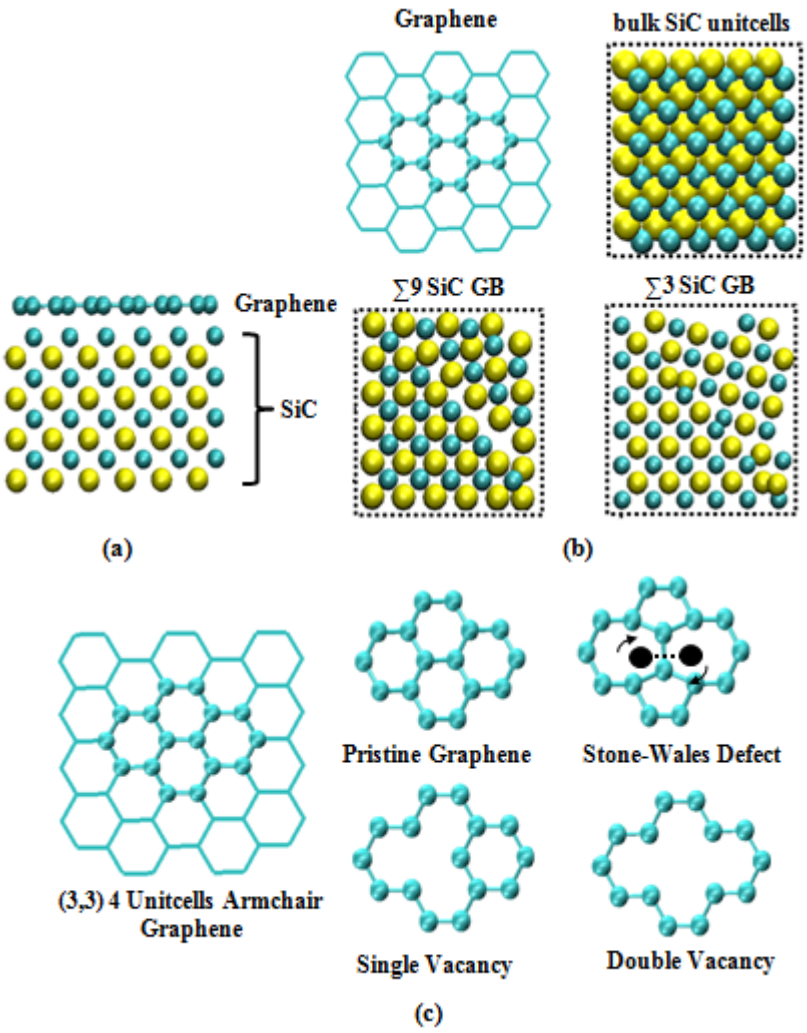

Figure 40. A schematic of examined epitaxial graphene on 3C-SiC nanostructure.

We consider two GB configurations such as ∑ 9{110}<001> tilt GB and ∑ 3{110}<001> tilt GB shown in Fig. 40 (b) for SiC substrates. Four different graphene defect types (pristine graphene, Stone-Walls defect, single vacancy, and double vacancy), commonly observed defects in graphene structures, are shown in Fig.40 (c). The tensile test was performed based on *ab initio* electronic structure calculations using the Car-Parrinello molecular dynamics (CPMD) framework within the density functional theory.

Figure 41 shows the stress and strain relations of the EG on SiC as a function of defect types and SiC GB configurations. For all examined graphene nanostructures, the EG on bulk SiC has the highest value of tensile strength, and the one on ∑ 9 tilt SiC GB comes in the second while the one on ∑ 3 tilt SiC GB shows the lowest peak tensile strength. It is also shown in Fig. 41 that the peak tensile strength of EG decreases in the presence of graphene defect: among the EG with defect, the EG with Stone-Walls defect has the highest tensile strength, and the ones with single vacancy and double vacancy comes the second and third, respectively. It is interesting to note that the grain boundary configuration of the SiC substrate plays more crucial role than the type of graphene defect in tensile strength of EG on SiC.

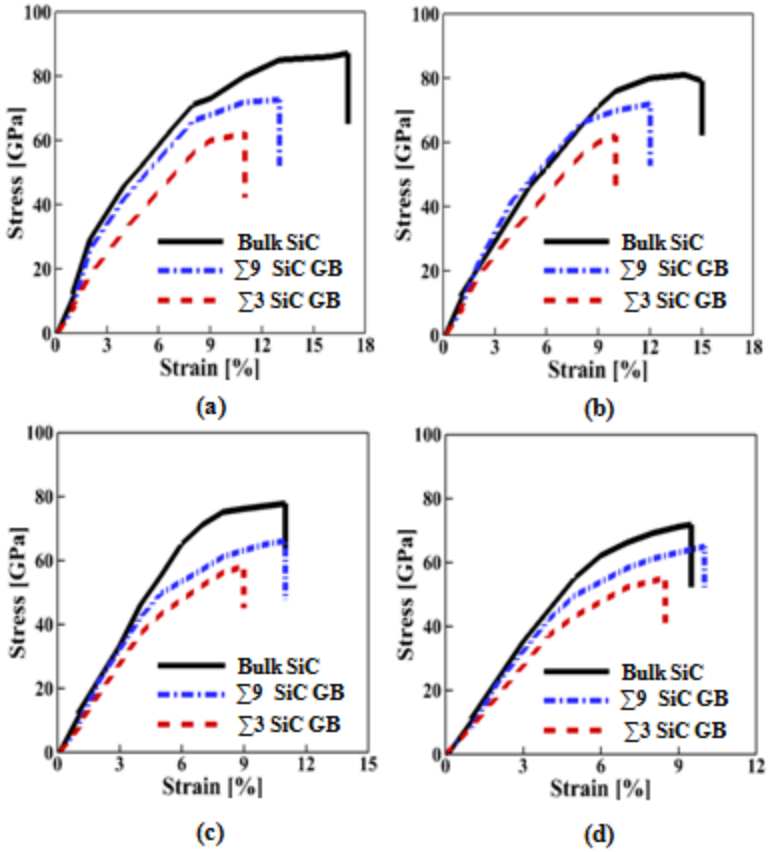

Figure 41. Peak tensile strength of examined epitaxial graphene nanostructures with an account of four different defect types: (a) the pristine graphene, (b) the graphene with Stone-Walls defect, (c) the graphene with single vacancy, and (d) the graphene with double vacancy.

It is well established that potential energy is inversely related to the bond strength of an atomic system. In order to examine the bond strength of the examined EG nanostructures, the potential energy values were analyzed as a function of SiC substrate GB configuration and graphene defect type. For comparison purposes, potential energy value for pristine graphene without SiC substrate is used as the reference value (i.e. E_0 = -136.55 eV/atom). The values of potential energy for each EG nanostructure were subtracted by the reference value and are plotted in Fig. 42 as a function of tensile strain. Potential energy of the EG nanostructure increases in the presence of graphene defect and SiC substrate GBs. For the same SiC GB configuration, pristine graphene has the lowest potential energy and the one with the Stone-Walls defect comes the next, while graphene with double vacancy has the highest potential energy.

The potential energy analyses so far explain why peak tensile strength of the examined nanostructures decreases in presence of SiC GBs and graphene defects. Because the bond strength decreases in presence of GB and graphene defects, the peak tensile strength also decreases under such cases. It is also interesting to note from Fig. 41 that peak tensile strength of EG nanostructures also follows such trend. This shows the influence of strong interaction between graphene and SiC substrate on peak tensile strengths of graphene.

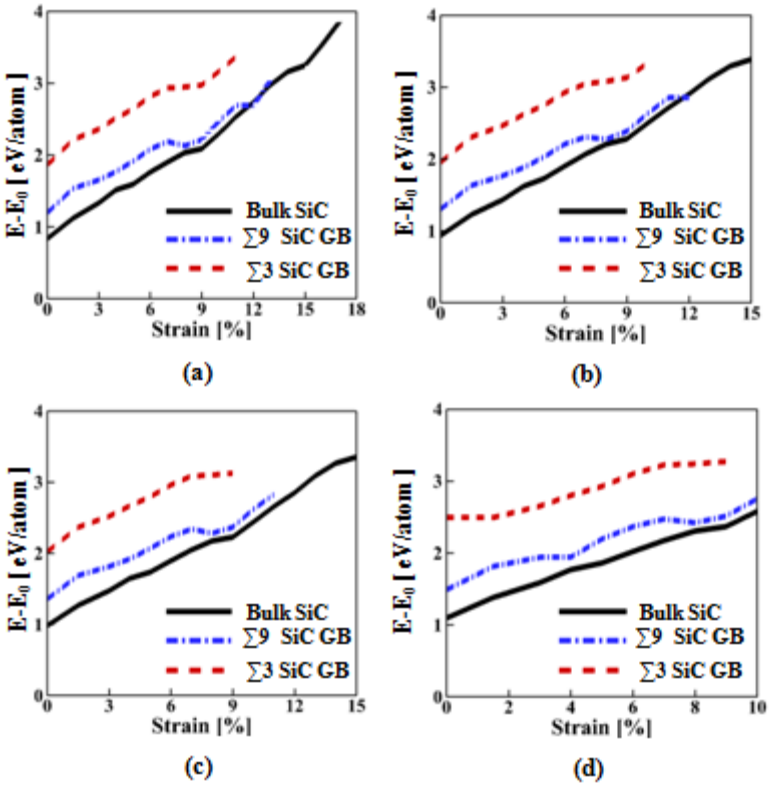

Figure 42. The potential energy of the examined EG nanostructures with an account of four different defect types: (a) the pristine graphene, (b) the graphene with Stone-Walls defect, (c) the graphene with single vacancy, and (d) the graphene with double vacancy. E_0 is the potential energy of pristine graphene without SiC substrate.

PATENTS, PUBLICATIONS AND PRESENTATIONS

PATENTS

1. Invention Disclosure: Battelle File No. 30705-E, DOE Docket No. S-123,972 (ORO) titled "Controlled Polytypes in SiC". For the same invention disclosure, the University of Washington Reference No. is 47168.

PUBLICATIONS

1. S. Arreguin, and R. K. Bordia. "Precursor Derived Nanostructured Si-C-X Materials for Nuclear Applications." *Transactions of the American Nuclear Society* **106** (2012): 107-108.
2. Y. S. Han and V. Tomar, "An ab-initio study on the peak tensile strength of tungsten with an account of helium point defects", *International Journal of Plasticity* **48** (2013): 54-71
3. Y. Han, and V. Tomar, "An ab-initio analysis of the influence of knock-on atom induced damage on the peak tensile strength of 3C-SiC grain boundaries", *International Journal of Damage Mechanics*, doi:10.1177/1056789514540315 (2014).
4. Y. Han, and V. Tomar, "An ab-initio investigation of the effect of graphene on the strength-electron density correlation on SiC grain boundaries", *Computational Material Science*, Volume **92**, Pages 422-430 (2014).

5. O. Flores, R.K. Bordia, D. Nestler, W. Krenkel, G Motz, **"**Ceramic fibers based on SiC and SiCN systems: Current research, development, and commercial status", *Advanced Engineering Materials*, **16** [6], p 621-636, (2014).
6. K. Wang, J. Unger, J.D. Torrey, B.D. Flinn and R.K. Bordia, "Corrosion resistant polymer derived ceramic composite environmental barrier coatings", *Journal of the European Ceramic Society*, **34**[12] 3597-3606 (2014).
7. T. Konegger, J. Torrey, O. Flores, T. Fey, B. Ceron-Nicolat, G. Motz, F. Scheffler, M. Scheffler, P. Greil and R. K. Bordia, "Ceramics for Sustainable Energy Technologies with a Focus on Polymer-Derived Ceramics", in *Novel Combustion Concepts for Sustainable Energy Development*, **Eds. A.K. Agarwal, A. Pandey, A.K. Gupta, S.K. Agarwal and A. Kushari**, 501-533 Springer India (December 2014).
8. S. Arreguin, R.K. Bordia, and C.H. Henager, Jr., 2014, Polytypic Stabilization of Nanostructured Polymer Derived SiC for Nuclear Applications, Accepted for publication in the American Nuclear Society Transactions 2014 Winter Meeting.

PRESENTATIONS

1. Shelly Arreguin and R.K. Bordia, "Precursor derived SiC-X ceramics for high-temperature nuclear applications", Student Session, American Nuclear Society, Hollywood Beach, FL, June 2011.
2. Arreguin, S., Bordia, R.K., Materials Science & Technology Precursor Derived SiC-X Materials for next Generation Nuclear Applications, Material Science Challenges for Nuclear Applications: Nanostructured Materials**,** October 2011, Columbus, OH.
3. Han, Y.S., and Tomar*, V., 2011, "Interface affected cascading in nuclear materials and its correlation with bond strength," ASME 2011 International Mechanical Engineering Congress & Exposition, November 11-17, 2011, Denver, CO.
4. Han, Y.S., and Tomar*, V., 2012, "Correlating fractal dimensionality with nuclear cascading failure," , Materials Science & Technology 2012 Conference & Exhibition, October 07-11, 2012 | Pittsburgh, Pennsylvania. (**invited**).
5. Arreguin, S. and Bordia, R.K., "SiC Ceramics for Next Generation Nuclear Applications" 2nd Annual Science & Policy Summit University of Washington Seattle
6. Arreguin, S. and Bordia, R.K., Polymer Derived SiC for Nuclear Applications, Sao Carlos Advanced School for Materials Science & Engineering Ceramic Symposium, Sao Carlos, Brazil, March 2012
7. Arreguin, S. and Bordia, R.K., "Precursor Derived Si-C-X Materials for Nuclear Applications" (abstract published in the ANS transactions), American Nuclear Society, Chicago, IL, Research by US-DOE Sponsored Students, June 2012
8. Arreguin, S. and Bordia, R.K., Precursor Derived SiC Ceramics for Next Generation Nuclear Applications, MS&T, Columbus, OH, Material Science Challenges for Nuclear Applications: Nanostructured Materials**,** October 2011.
9. Han, Y.S, and Tomar, V., 2014, "Computational Study of the irradiation dependent failure in SiC" Society of Engineering Science Meeting, 2014 Annual Meeting, 1-3 Oct 2014, West Lafayette-IN

10. G. Motz and R.K. Bordia, "Ceramic Fibers: Review of the Current Status and Recent Developments" International Symposium on Fibers Interfacing the World, October 2013, Clemson, SC (**Invited)**.
11. R. K. Bordia, "Role of Ceramics in Addressing the Energy Challenge: Research in Bordia Group", International Workshop on Novel Combustion Concepts for Sustainable Energy Development, Indian Institute of Technology, January 2014, Kanpur, INDIA (**Invited)**
12. R.K. Bordia, "Polymer Derived Composite Ceramic Coatings and Joints: Processing, Properties and Performance", Université de Grenoble - Alpes, SIMAP Laboratory, CNRS, June 2014, Grenoble, FRANCE (**Invited)**.
13. R.K. Bordia, "SiC/SiC Composites: Creep and Environmental Barrier Coatings", Workshop on Testing and Modeling Ceramic and Carbon Matrix Composites, June 2014, Cachan, FRANCE (**Invited)**.
14. R.K. Bordia, K. Wang, R. Riedel and E. Ionescu, "Amorphous and Nanostructured Ceramics from Silicon-Based Molecular Precursors", International Symposium on Metastable, Amorphous and Nanostructured Materials, July 2014 Cancun, MEXICO **(Plenary)**.
15. G. Motz and R.K. Bordia, "Processing, Properties and Performance of Precursor Derived Si-N Based Coatings", ISNT 2014, Wildbad Kreuth, GERMANY, August 2014 (**Invited)**.
16. S. Arreguin, R. K. Bordia and C. H. Henager, Jr., American Nuclear Society, Winter Meeting, Anaheim, CA *Structural Materials and Used Nuclear Fuel Disposition,* November 2014.
17. M. Stackpoole, K. Wang and R.K. Bordia, "Precursor Derived Ceramic Joints for Ceramics and Ceramic Matrix Composites", 39th International Conference and Exposition on Advanced Ceramics and Composites, Daytona Beach, FL, January 2015 (**Invited)**.

MILESTRONE STATUS AND STUDENTS AND POST-DOCS SUPPORTED

MILESTONE STATUS

MI: Selection of polymers, processing parameters, minor upgrade to equipment
Has been completed (2/15/2011)

M2: Detailed protocols for the processing studies
Has been completed (6/15/2011).

M3: Establishing the simulation microstructures in accordance with experiments
Has been completed (3/31/2011).

M 4: Establish the protocols for high temperature stability and creep studies
Has been completed (9/30/2012).

M 5: Establish the protocols for experimental radiation and design of irradiation specimen and mask effect studies
Has been completed (11/30/2013).

M6: Establishing the protocol for simulation of the microstructures
Has been completed (9/30/2011).

M 7: Preliminary mechanical properties, high temperature stability and creep studies
Has been completed (8/26/14).

M8: Establishing the protocol for simulation of the effect of radiation
Has been completed (12/31/2011)

M 9: Preliminary experimental radiation damage studies to qualify the protocols

Has been completed (8/26/14).

M 10: Processing studies completed and a set of compositions identified for radiation effect and high temperature properties studies
Has been completed (3/31/2014)

M11: Preliminary finding of effect of irradiation on nanostructure stability
Has been completed (8/26/14).

M12: Initial parametric simulation studies on effect of radiation on nanostructure
Has been completed (9/30/2012).

M13: Complete the high temperature stability studies
Has been completed (8/26/14).

M14: Complete the mechanical characterization including creep studies
Has been completed (8/26/14).

M15: Radiation damage studies completed including inert gas mobility. Identification of the most promising compositions and processing parameters.
Has been completed (8/26/14).

M 16: Establishing correlation between experimental and simulation based studies of radiation effects
Has been completed (8/26/14)

STUDENTS AND POST – DOCTORAL RESEARCH ASSOCIATES:

Support from this project has partially funded the education and training of the following students and post-doctoral research associates.

Name	**Citizenship**	**Degree or Degree Seeking**	
You Sung Han	South Korea	Seeking PhD	
Kevin Strong	United States	Seeking PhD	
Shelly Arreguin	United States	Seeking Ph.D.	
Dr. Kaishi Wang	China	Post Doctoral Research Associate	